TOMOGRAPHIC ESTIMATION OF THE POINT-SPREAD FUNCTION OF AN ULTRASOUND IMAGING SYSTEM FOR DECONVOLUTION

J. K. H. Ng, R. W. Prager, N. G. Kingsbury,
G. M. Treece and A. H. Gee

CUED/F-INFENG/TR 529

28 June 2005

University of Cambridge
Department of Engineering
Trumpington Street
Cambridge CB2 1PZ
United Kingdom

Email: jkhn2/rwp/ngk/gmt11/ahg @eng.cam.ac.uk

Tomographic Estimation of the Point-Spread Function of an Ultrasound Imaging System for Deconvolution

James Ng, Richard Prager, Nick Kingsbury, Graham Treece, Andrew Gee

University of Cambridge, Department of Engineering,

Trumpington Street, Cambridge CB2 1PZ

Abstract

The usefulness of ultrasound images in medical diagnostics is limited by inherent blurring and consequent poor image resolution. Algorithms that attempt to correct this blur generally require knowledge of the imaging system's *point-spread function* (PSF). In this report, we introduce a method for determining the three-dimensional PSF of an ultrasound imaging system by acquiring images of a line target and applying tomographic reconstruction methods. We show that imaging a line target yields the projection of the PSF along the axis of the target, and given a sufficient number of projections at different angles, we can reconstruct the PSF tomographically, e.g. by using the filtered backprojection method. We discuss some of the practical considerations that need to be addressed when preparing a suitable line target phantom. Our experimental results show that the PSF estimated in this way has good fidelity to its theoretically predicted counterpart. We also include results of frequency-domain deconvolution with Tikhonov regularisation which show modest improvement in resolution as measured by the widths of the corresponding two-dimensional autocorrelation functions.

1 Introduction

Pulse-echo ultrasound imaging is now a common tool in medical diagnostics. In standard clinical use, an ultrasound image is acquired by using a probe to transmit high frequency acoustic waves into the subject and to then listen for echoes. The acquired radio-frequency (RF) traces can, after postprocessing, be interpreted as an image of the subject's acoustic *reflectivity* which is strongly correlated with structural features. Compared to other imaging modalities, pulse-echo ultrasound imaging enjoys several advantages: it does not expose the subject to harmful radiation; acquisition is fast enough for real-time display; and the required equipment is relatively cheap to obtain. These advantages, however, come at the price of inherent blurring and loss of resolution. Correcting this requires proper characterisation of the blurring.

It is well-known that, in the case of weak scattering (i.e. when the amplitude of the reflected echoes is much smaller than the amplitude of the incident waves), the first Born approximation holds and

the imaging process can be modelled as a linear system [1, 2, 3, 4]. Any linear imaging system can be characterised by a *point-spread function* (PSF) which models the spatial extent of the blurring of a single point. Accurate knowledge of this PSF is essential for blur removal and resolution enhancement. If the mechanics and geometry of the probe are accurately known, then this PSF can be calculated; otherwise, it has to be experimentally determined. A naive experimental method would be to simply image a point target. Physical manipulation of a sufficiently small target, however, is in practice near impossible, and the reflections obtained are usually too weak and too heavily corrupted by noise to be of any significant use. A more practical approach, which we describe in this report, is to image a line target (e.g. a very thin wire) at different orientations and to use tomographic methods to reconstruct the PSF.

The use of line targets in the characterisation of acoustic fields is not unique to this paper. Raum and O'Brien [5] proposed using reflections from line targets to determine the spatial and temporal extents of acoustic fields. A more sophisticated tomographic procedure was described by Li *et al.* [6] to reconstruct the two-dimensional distribution of acoustic intensity in the focal plane of an ultrasonic pulse-echo system. We extend the work of Li *et al.* by computing, not just a two-dimensional distribution at the focal plane, but the entire three-dimensional PSF which can be used in subsequent image restoration algorithms. We also include some deconvolution results obtained with both our tomographically reconstructed PSF and a theoretically calculated PSF.

2 Theory

We adopt a rectangular coordinate system as shown in Figure 1(a), where the z axis is parallel to the direction of wave propagation. The probe captures a two-dimensional RF image parallel to the xz plane; a three-dimensional dataset is obtained by translating the probe in the y direction and capturing multiple parallel two-dimensional RF images. We shall use the terms *lateral*, *elevational* and *axial* to refer to directions parallel to the x, y and z axes respectively. We shall also use t to denote time.

It is explicity shown in [4] that, in such a coordinate system, the PSF is shift-variant only in the axial direction. We may therefore express the imaging process by the Fredholm integral,

$$\begin{aligned} g(x,y,t) &= \iiint h(x-x', y-y', z', t)\, f_m(x', y', z')\, dx'\ dy'\ dz' \\ &= \iiint h(x', y', z', t)\, f_m(x-x', y-y', z')\, dx'\ dy'\ dz' \end{aligned} \tag{1}$$

where $g(x,y,t)$ is the three-dimensional RF image, $h(x,y,z,t)$ is the axially shift-variant PSF and $f_m(x,y,z)$ is the reflectivity. The integration is taken over three-dimensional space.

We position a line target at an axial depth z_0 (i.e. in the plane $z = z_0$) and orient it at an angle θ to the y axis. The line target effectively behaves as a two-dimensional impulse function and causes the PSF to be integrated along its axis (we shall refer to the result of this integration as the *projection* of the PSF). To demonstrate this formally, we introduce in Figure 1(b) a new set of axes labelled x_p and y_p which are simply the x and y axes rotated anticlockwise through an

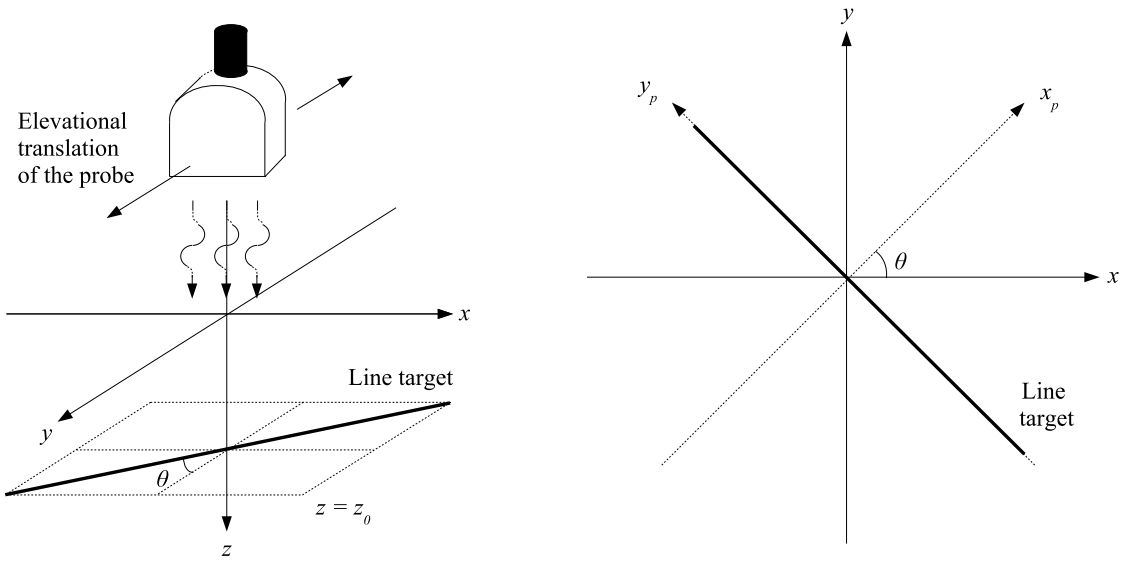

(a) Perspective view.

(b) Bird's eye view.

Figure 1: Apparatus setup for measurement of the PSF.

angle θ; the line target now lies conveniently on the y_p axis. The (x, y) coordinates and (x_p, y_p) coordinates of a point are related via

$$\begin{bmatrix} x_p \\ y_p \end{bmatrix} = \begin{bmatrix} \cos\theta & \sin\theta \\ -\sin\theta & \cos\theta \end{bmatrix} \begin{bmatrix} x \\ y \end{bmatrix} \Longleftrightarrow \begin{bmatrix} x \\ y \end{bmatrix} = \begin{bmatrix} \cos\theta & -\sin\theta \\ \sin\theta & \cos\theta \end{bmatrix} \begin{bmatrix} x_p \\ y_p \end{bmatrix} \tag{2}$$

We have $h(x, y, z, t) = h(x_p \cos\theta - y_p \sin\theta, x_p \sin\theta + y_p \cos\theta, z, t)$ and $f_m(x, y, z) = \delta(x_p)\,\delta(z - z_0)$. Expressing the Fredholm integral of Equation 1 in terms of x_p and y_p, we obtain

$$g(x, y, t) = \iiint h(x' \cos\theta - y' \sin\theta, x' \sin\theta + y' \cos\theta, z, t)\,\delta(x_p - x')\,\delta(z' - z_0)\,dx'\;dy'\;dz' \tag{3}$$

and, after simplifying this integral and writing $g(x, y, t) = g_{z_0}(x_p, \theta, t)$, we obtain as required

$$g_{z_0}(x_p, \theta, t) = \int h(x_p \cos\theta - y_p \sin\theta, x_p \sin\theta + y_p \cos\theta, z_0, t)\,dy_p = \int h(x, y, z_0, t)\,dy_p \tag{4}$$

For a fixed value of t, the quantity $g_{z_0}(x_p, \theta, t)$ is the Radon transform of $h(x, y, z_0, t)$, and there are a number of ways of reconstructing $h(x, y, z_0, t)$ from $g_{z_0}(x_p, \theta, t)$. In our work, we chose to use the well-known *filtered backprojection* method [7, chapter 3].

The filtered backprojection method recovers an image from its projections by applying a reconstruction filter to each projection and then integrating the projections over 180°. We may express this formally by writing

$$h(x, y, z_0, t) = \frac{1}{2\pi} \int_0^{\pi} g_{z_0}(x_p, \theta, t) * r(x_p)\,d\theta \tag{5}$$

where $r(x_p)$ is the impulse response of a reconstruction filter with frequency response $\widehat{r}(k) = |k|$ and k is the angular frequency associated with x_p. Strictly speaking, the frequency response $|k|$ is divergent and its inverse Fourier transform does not exist. We can overcome this by windowing the frequency response to bandlimit it [7].

3 Method

Our procedure for estimating the PSF at a particular axial depth can thus be summarised as follows. A line target is first positioned at the required axial depth. Three-dimensional RF images of the line target, rotated at equal angular increments through a total of 180°, are then acquired. Each three-dimensional RF image is then averaged along the axis of the line target to obtain a good estimate of $g_{z_0}(x_p, \theta, t)$. Finally, for each time sample (i.e. each value of t), Equation 5 is applied to reconstruct $h(x, y, z_0, t)$.

There are a number of practical considerations that we shall now address. For a valid estimate of the PSF to be obtained, the scattering must be weak. Standard results for acoustic scattering from cylinders [8, chapter 8] suggest that the amplitude of scattered waves is dependent on the cylinder's diameter, and that the scattered wave has much smaller amplitude than the incident wave if the cylinder's diameter is small compared to the wavelength, irrespective of the cylinder's material properties.

Another important factor to consider is the speed of sound of the medium surrounding the line target. Most medical ultrasound units assume a constant speed of sound of 1540m/s (the average speed of sound in human tissue) for electronic focussing. Andersen and Trahey [9] showed that an error as small as 5% in the speed of sound can lead to quite significant aberrations in the measured PSF. It is therefore important to embed the line target in an acoustically homogeneous medium with the correct speed of sound.

4 Results

In our experiments, we used a Dynamic Imaging Diasus ultrasound machine with a 6.5MHz probe. The probe surface consisted of 128 piezoelectric elements, each measuring 0.3mm (lateral) by 0.6mm (elevational) with a lateral gap of 0.025mm between elements. The lateral and elevational focal lengths were 21mm and 23mm respectively. The RF data was acquired at a sampling rate of 66.6MHz.

We constructed a phantom consisting of a tungsten wire with a diameter of 0.01mm embedded in a tissue-mimicking medium consisting mainly of glycerol, water and agar[1]. The speed of sound in the medium was measured to be within 1% of the nominal 1540m/s. The line target was placed at the elevational focus. During acquisition, the probe was translated in elevational increments of 0.05mm. Projections of the PSF were acquired at angular increments of 5°. We applied the Shepp-Logan reconstruction filter to each projection, which has the $|k|$ frequency response multiplied by a rectangular window and weighted by a sine function (this reduces ringing artifacts [7]).

[1] Recipe provided by the Department of Medical Physics, University of Edinburgh.

For benchmarking purposes, we also computed the theoretical PSF by simulating the response of a point target under the same conditions using Field II [10]. We present our results in Figure 2, where we have displayed cross-sections of the tomographically reconstructed PSF and the theoretical PSF after envelope detection and normalisation. The cross-sections show the tomographically reconstructed PSF to be in good agreement with its theoretical counterpart.

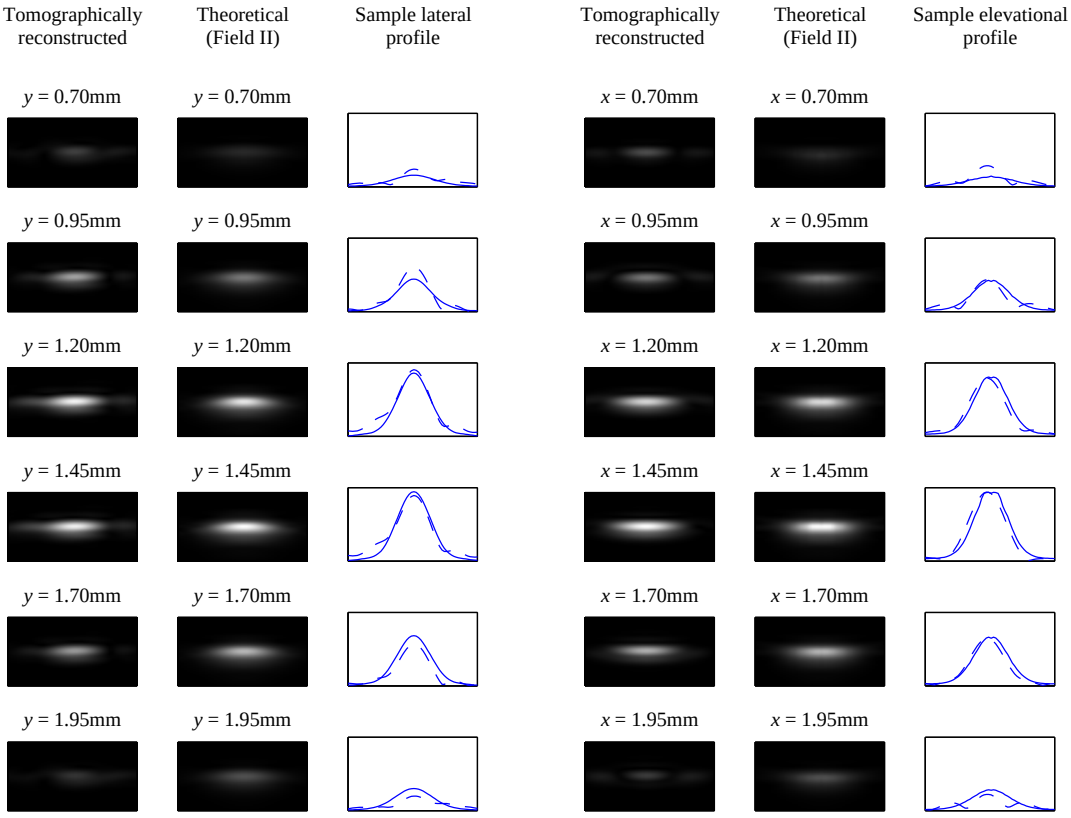

(a) Axial-lateral cross-sections (the axial direction is vertical). The dashed lines correspond to the tomographically reconstructed PSF.

(b) Axial-elevational cross-sections (the axial direction is vertical). The dashed lines correspond to the tomographically reconstructed PSF.

Figure 2: Cross-sections of the reconstructed and theoretical PSFs. Each cross-section measures 1.5μs (1.16mm) by 2.2mm.

5 Deconvolution

Subsequently, we used the tomographically reconstructed and theoretical PSFs to deconvolve a three-dimensional dataset of a spherical void, 2mm in diameter, embedded in tissue-mimicking material. To perform this deconvolution, we have assumed that the PSF is approximately shift-invariant (which is reasonable over a small axial distance) and that the the signal is corrupted by

additive white Gaussian noise $n(x, y, t)$, i.e.

$$g(x, y, t) = h(x, y, t) * f_m(x, y, t) + n(x, y, t) \tag{6}$$

We applied Tikhonov regularisation in the frequency domain, which amounts to filtering the dataset by a deconvolution filter with transfer function

$$T(\mathbf{k}) = \frac{H^*(\mathbf{k})}{|H(\mathbf{k})|^2 + \tau} \tag{7}$$

where $\mathbf{k}$ is the angular frequency corresponding to (x, y, t), $H(\mathbf{k})$ is the Fourier transform of $h(x, y, t)$ and τ is a regularisation parameter. This is equivalent to applying a Wiener filter assuming a constant signal-to-noise ratio (SNR) of $\frac{1}{\tau}$.

The results of deconvolution with $\tau = 0.1$ and $\tau = 0.05$ are displayed in Figures 3 and 4. To quantify the degree of deconvolution achieved, we have included plots from the two-dimensional autocorrelation functions of selected cross-sections from the original and deconvolved datasets. The reductions in the lateral and elevational widths of these autocorrelation functions after deconvolution are tabulated in Table 1.

Table 1: Reductions in the widths of the autocorrelation functions after deconvolution.

	$\tau = \mathbf{0.1}$	$\tau = \mathbf{0.05}$
Lateral reduction (see Figures 3(b) and 4(b))		
Deconvolution with tomographic PSF	14.6%	13.4%
Deconvolution with simulated PSF	7.1%	14.1%
Elevational reduction (see Figures 3(d) and 4(d))		
Deconvolution with tomographic PSF	26.0%	37.0%
Deconvolution with simulated PSF	15.91%	17.0%

6 Conclusions and Discussion

In this report, we have presented a feasible method for estimating the PSF of an ultrasound imaging system via tomographic reconstruction from acquired reflections off a line target. Such an approach is a viable and accurate alternative when a lack of knowledge of the transducer's mechanical and geometric properties prevents the PSF from being computed theoretically. An estimate of the PSF is required for blur removal and resolution enhancement and we envisage the possibility of our PSF estimation procedure being used as an auxiliary tool in image restoration algorithms.

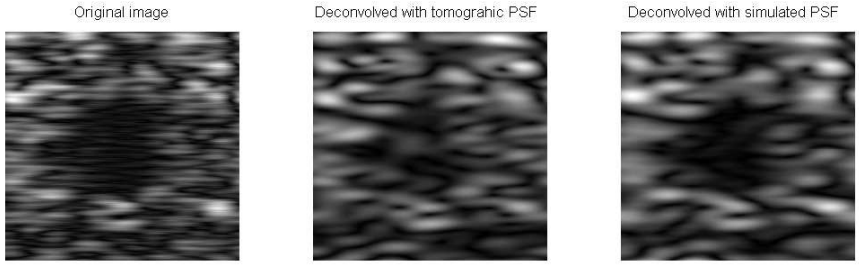

(a) Axial-lateral cross sections.

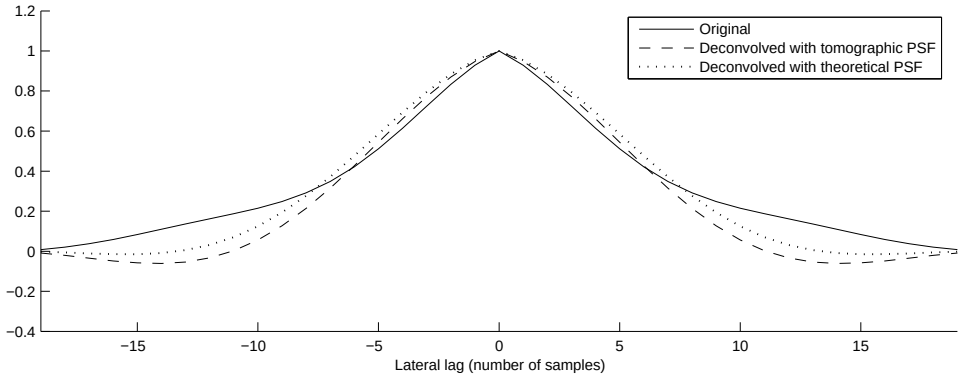

(b) Selected lateral profile from the 2D autocorrelation functions of (a).

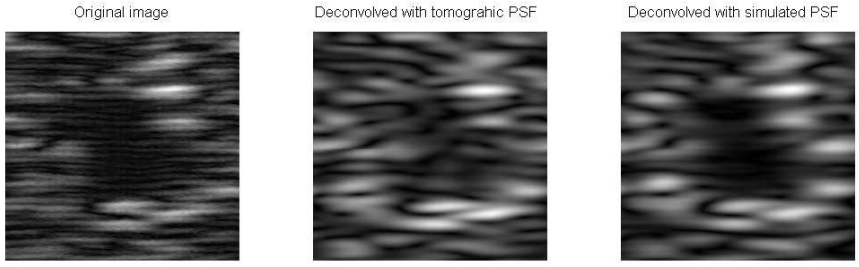

(c) Elevational cross-sections.

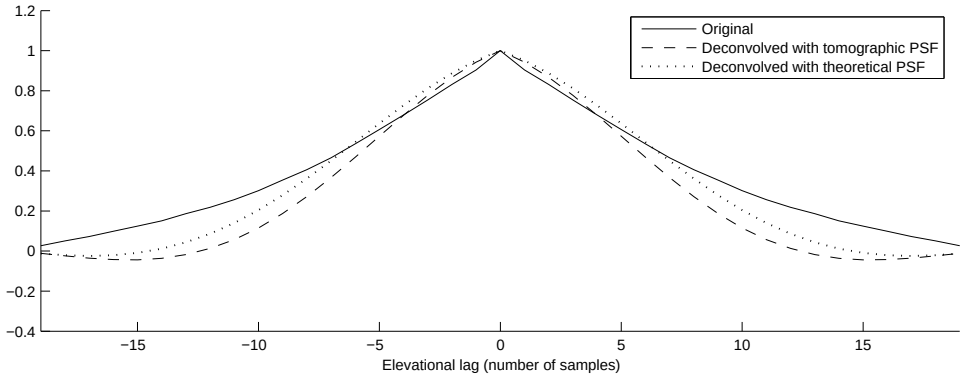

(d) Selected elevational profile from the 2D autocorrelation functions of (c).

Figure 3: Deconvolution results for $\tau = 0.1$ (equivalent SNR = 10dB). Each cross-section measures 5.20μs (4mm) by 4mm.

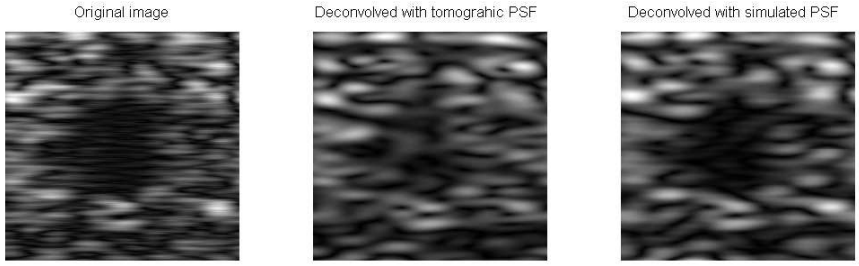

(a) Axial-lateral cross sections.

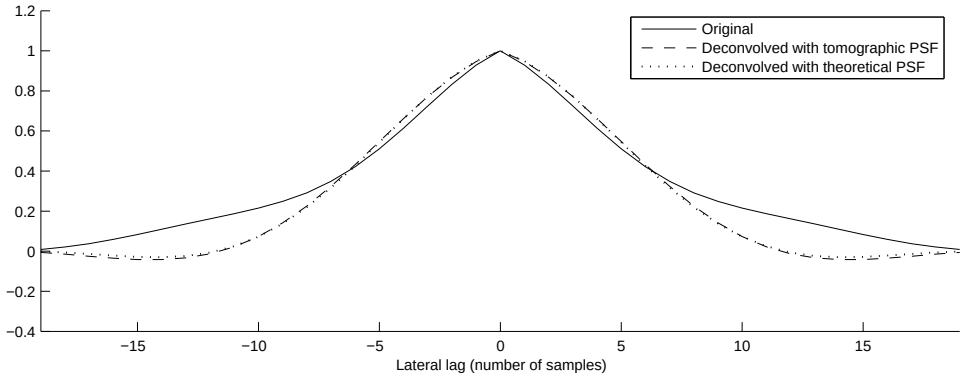

(b) Selected lateral profile from the 2D autocorrelation functions of (a).

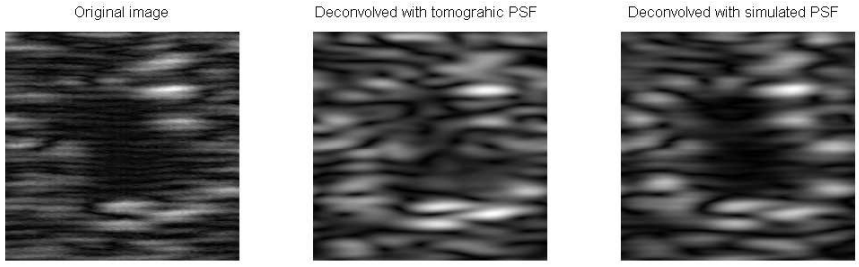

(c) Elevational cross-sections.

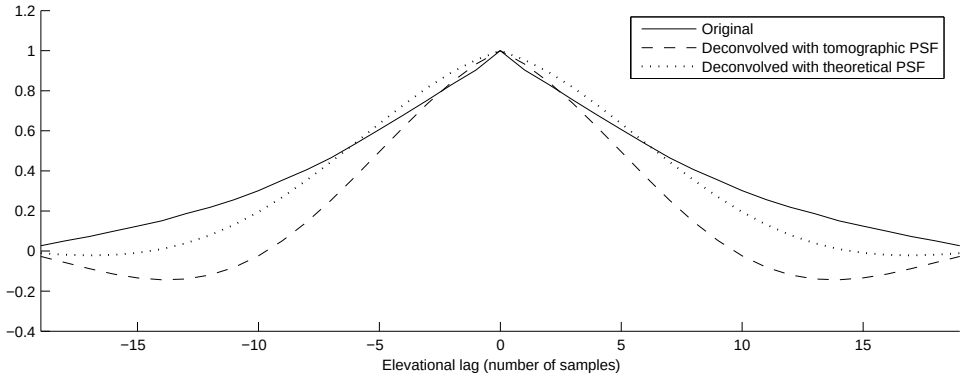

(d) Selected elevational profile from the 2D autocorrelation functions of (c).

Figure 4: Deconvolution results for $\tau = 0.05$ (equivalent SNR = 13dB). Each cross-section measures 5.20μs (4mm) by 4mm.

Our attempt at deconvolution by applying frequency domain Tikhonov regularisation resulted in modest improvements in image quality. It is encouraging to observe that in all the deconvolved datasets, the best improvement was observed in the elevational direction, since elevational blurring is usually the most severe. Wiener-type deconvolution filters (such as the one we used) are known to be optimal only for signals with Gaussian statistics, and since the tissue reflectivity is unlikely to obey Gaussian statistics, we expect better deconvolution to be achieved by techniques which impose more appropriate statistical priors on the tissue reflectivity.

The source files and data files for the results presented in this report may be downloaded at http://www-sigproc.eng.cam.ac.uk/~jkhn2/PSFFromWire.

References

[1] J. C. Gore & S. Leeman. "Ultrasonic backscattering from human tissue: a realistic model." *Physics in Medicine and Biology* **22(2)**, pp. 317–326, 1977.

[2] J. A. Jensen. "A model for the propagation and scattering of ultrasound in tissue." *Journal of the Acoustical Society of America* **89(1)**, pp. 182–190, January 1991.

[3] R. J. Zemp, C. K. Abbey & M. F. Insana. "Linear system models for ultrasonic imaging: application to signal statistics." *IEEE Transactions on Ultrasonics, Ferroelectrics and Frequency Control* **50(6)**, pp. 642–654, June 2003.

[4] J. K. H. Ng, R. W. Prager, N. G. Kingsbury et al. "Modelling ultrasound imaging as a linear, shift-variant system." Technical Report CUED/F-INFENG/TR 509, Cambridge University Engineering Department, January 2005.

[5] K. Raum & W. D. O'Brien, Jr. "Pulse-echo field distribution measurement technique for high-frequency ultrasound sources." *IEEE Transactions on Ultrasonics, Ferroelectrics and Frequency Control* **44(4)**, pp. 810, July 1997.

[6] T.-B. Li, H. Shimamoto & M. Ueda. "Measurement of transmit-receive sound intensity pattern of ultrasound transducer using echoes scattered by a fine wire." *Journal of the Acoustical Society of Japan* **46(10)**, pp. 810, 1990.

[7] Z.-H. Cho, J. P. Jones & M. Singh. *Foundations of Medical Imaging.* John Wiley and Sons, 1993.

[8] P. M. Morse & K. U. Ingard. *Theoretical Acoustics.* International Series in Pure and Applied Physics. McGraw-Hill Book Company, 1968.

[9] M. E. Anderson & G. E. Trahey. *A seminar on k-space applied to medical ultrasound*, April 2000. Available: http://dukemil.egr.duke.edu/Ultrasound/k-space/bme265.htm [2005, March 29].

[10] J. A. Jensen. "Field: a program for simulating ultrasound systems." In *Proceedings of the 10th Nordic-Baltic Conference on Biomedical Imaging, Medical and Biological Engineering and Computing in Tampere*, volume 34, pp. 351–353. 1996.